Targeting Cancer Cells by Novel Engineered Modular Transporters

Dinara G. Gilyazova,[1,2] Andrey A. Rosenkranz,[1,2] Pavel V. Gulak,[1] Vladimir G. Lunin,[1,3] Olga V. Sergienko,[3] Yuri V. Khramtsov,[1] Kirill N. Timofeyev,[2] Mikhail A. Grin,[4] Andrey F. Mironov,[4] Andrey B. Rubin,[2] Georgii P. Georgiev,[1] and Alexander S. Sobolev[1,2]

[1]Institute of Gene Biology, Russian Academy of Sciences; [2]Biological Faculty, Moscow State University; [3]Gamaleya Institute of Epidemiology and Microbiology, Russian Academy of Medical Sciences; and [4]Moscow State Academy of Fine Chemical Technology, Moscow, Russia

Abstract

A major problem in the treatment of cancer is the specific targeting of drugs to these abnormal cells. Ideally, such a drug should act over short distances to minimize damage to healthy cells and target subcellular compartments that have the highest sensitivity to the drug. We describe the novel approach of using modular recombinant transporters to target photosensitizers to the nucleus, where their action is most pronounced, of cancer cells overexpressing ErbB1 receptors. We have produced a new generation of the transporters consisting of (*a*) epidermal growth factor as the internalizable ligand module to ErbB1 receptors, (*b*) the optimized nuclear localization sequence of SV40 large T-antigen, (*c*) a translocation domain of diphtheria toxin as an endosomolytic module, and (*d*) the *Escherichia coli* hemoglobin-like protein HMP as a carrier module. The modules retained their functions within the transporter chimera: they showed high-affinity interactions with ErbB1 receptors and α/β-importin dimers and formed holes in lipid bilayers at endosomal pH. A photosensitizer conjugated with the transporter produced singlet oxygen and ·OH radicals similar to the free photosensitizer. Photosensitizers-transporter conjugates have >3,000 times greater efficacy than free photosensitizers for target cells and were not photocytotoxic at these concentrations for cells expressing a few ErbB1 receptors per cell, in contrast to free photosensitizers. The different modules of the transporters, which are highly expressed and easily purified to retain full activity of each of the modules, are interchangeable, meaning that they can be tailored for particular applications. (Cancer Res 2006; 66(21): 10534-40)

Introduction

The creation of special macromolecular systems for targeted cell-specific intracellular drug delivery is a necessary step in the development of effective drugs that treat cancer. Such drugs need to be transported only to specific or most vulnerable intracellular compartments where the effect of the drugs can be revealed. Although nucleic acids and polypeptides have been used in this approach, the most promising compounds are photosensitizers and radionuclides emitting short-range radiation, such as α-particles. Photodynamic therapy is based on a predominant accumulation of photosensitizers in a tumor and subsequent irradiation of the tumor with light of appropriate wavelength (1, 2). Upon photoactivation, photosensitizers generate reactive oxygen species (ROS; singlet oxygen and free radicals, such as ·OH and $\cdot HO_2$), which are active principles of the photosensitizers and able to damage proteins, nucleic acids, lipids, and other cellular components. However, photodynamic therapy has several considerable limitations. First, photosensitizers are not cell-specific agents; that is, normal cells are also able to accumulate photosensitizers, which results in a number of negative side effects (e.g., prolonged skin and retina photosensitization). Second, large doses of photosensitizers are normally required for efficient tumor cell killing owing to their nonoptimal subcellular distribution. Photodynamic action of photosensitizers does not exceed tens of nanometers from the site of their subcellular localization because ROS have a very short mean range within the cell. Photosensitizers localize in the cytoplasm, whereas the most sensitive site to ROS is the cell nucleus (3, 4); thus, there is little doubt that photosensitizer antitumor efficiency will depend on the subcellular distribution of photosensitizers (3, 5).

One way to redirect photosensitizers within the cells is to employ modular polypeptide transporters possessing (*a*) an internalizable ligand module providing for target cell recognition and subsequent receptor-mediated endocytosis of the transporter by the cell; (*b*) an endosomolytic module ensuring escape of the transporter from endosomes; (*c*) a module containing a nuclear localization sequence (NLS) and thus enabling interaction of the transporter with importins, the intracellular proteins ensuring active translocation into the nucleus; and (*d*) a carrier module for attachment of the photosensitizers. The photosensitizers transported to the cell nucleus by the modular carriers proved to be several orders of magnitude more efficient than nonmodified, free photosensitizers (3, 4, 6–8). Recently (9), we have produced and characterized modular recombinant transporters (MRT) for photosensitizers according to the above scheme with α-melanocyte-stimulating hormone (MSH) as the internalizable ligand module. These MRTs delivered the photosensitizer to the nuclei of murine melanoma cells and provided for a greater (about 230-fold) photodynamic effect than a nonmodified photosensitizer. All their four modules turned out to be necessary to achieve maximal photosensitizer efficiency, cell specificity, and significant bacterial expression of the MRTs. More recently (10), we have shown that our modular transporters can be efficiently used for carrying such α-emitting radionuclides as astatine-211 to enhance their cytotoxic activity and impart cell specificity to them.

As mentioned, the nature of ligand module determines the type of target cells; thus, the approach may be applicable to a wide variety of cancer cell types, by using ligands recognized by receptors overexpressed on these cells [e.g., insulin-like growth factors (carcinomas and osteosarcomas; ref. 11), nerve growth

Note: Supplementary data for this article are available at Cancer Research Online (http://cancerres.aacrjournals.org/).

Experiments were carried out with the use of the equipment from the Center of collective usage of the unique instrumentation of the Institute of Gene Biology.

Requests for reprints: Alexander S. Sobolev, Department of Molecular Genetics of Intracellular Transport, Institute of Gene Biology, Russian Academy of Sciences, 34/5 Vavilov Street, 119334, Moscow, Russia. Phone: 7-495-135-3100; Fax: 7-495-135-4105; E-mail: sobolev@igb.ac.ru.

doi:10.1158/0008-5472.CAN-06-2393

factor (neuroblastomas, pancreatic cancer; ref. 12), epidermal growth factor (EGF; head-and-neck cancer, bladder cancer, breast cancer, etc.; ref. 13), somatostatin (neuroendocrine tumors; ref. 14), and the aforesaid MSH (a number of melanomas; ref. 15)].

Here, we describe the novel approach of using MRTs to target photosensitizers to the nucleus, where their action is most pronounced, of cancer cells overexpressing ErbB1 receptors. The MRTs consist of an internalizable ligand (EGF), a nuclear localization sequence, a carrier protein, and a translocation domain of diphtheria toxin. The MRT modules retained their functions: they showed high-affinity interactions with ErbB1 receptors and α/β-importin dimers, ensuring nuclear transport of NLS-containing proteins; they form holes in supported bilayers at endosomal pH. A photosensitizer conjugated with the MRT produce ROS similar to the free photosensitizer. Photosensitizers-MRT conjugates have >3,000 times greater efficacy than free photosensitizers for target cells and were not photocytotoxic at these concentrations for cells expressing a few ErbB1 receptors per cell in contrast to free photosensitizers, thus showing cell specificity imparted by the MRTs.

Materials and Methods

Cell cultures. The A431 human epidermoid carcinoma cells and murine NIH 3T3 fibroblasts were maintained in DMEM (Sigma, St. Louis, MO) supplemented with 10% FCS (Life Technologies, Carlsbad, CA) and gentamicin (50 μg/mL). All the cell lines were maintained at 37°C in a humidified atmosphere consisting of 5% CO_2 in air.

Production of MRT-encoding plasmids and expression and purification of MRTs. All molecular biological procedures, including DNA isolation, endonuclease cleavage, phosphorylation, ligation, cell transformation, PCR, and generation of the NLS, HMP, and DTox modules, were done according to standard protocols as previously described (9).

The EGF module was generated by PCR using the primers 5′-GGGGGCCCGGGATCCAATTCCGATAGCGAGTGTCCTC-3′ (forward) and 5′-CAAGGAGATGGATCCCAACAGTCCTCCGGACACGGGGCC-3′ (reverse) and plasmid DNA containing the cloned EGF (16).

The $(Gly\text{-}Ser)_5$ spacer was generated synthetically from the oligonucleotides. Each oligonucleotide chain (forward, 5′-GATCCCCGGGTTCTGGCTCCGGCTCTGGTTCCGGTTCTGGCGCCAGATCTA-3′ and reverse, 5′-AGCTTAGATCTGGCGCCAGAACCGGAACCAGAGCCGGAGCCAGAACCCGGG-3′) was phosphorylated separately.

Expression of the MRTs was carried out in *Escherichia coli* strain M15 (carrying plasmid pREP4) according to the QIAGEN (Hilden, Germany) protocol. The extent of MRT expression ranged from 20% to 30%. The cells were lysed in 10 mmol/L HEPES-NaOH (pH 7.5), 0.5 % Triton X-100, 1 mmol/L phenylmethanesulfonyl fluoride, 1.5 μg/mL aprotinin, 1 mg/mL lysozyme (all from Sigma); sonicated (40 kHz); and centrifuged (17,000 rpm, JA-20 Beckman rotor) for 25 minutes. The MRTs were purified on Ni-NTA-agarose (QIAGEN) according to the standard procedure. Then the MRTs were dialyzed against 10 mmol/L Na-phosphate buffer (pH 8) with 150 mmol/L NaCl. Protein purity was assayed with 10% PAGE according to Laemmli et al. (17).

Preparation of photosensitizer-MRT conjugates. Two photosensitizers, chlorin e_6 (Porphyrin Products, Inc., Logan, UT) and bacteriochlorin *p*, prepared according to Mironov et al. (18), were conjugated with the MRTs (1.1:1 molar ratio) using 1-ethyl-3-(3-dimethylaminopropyl)-carbodiimide and *N*-hydroxysuccinimide (both from Sigma). Conjugates were purified from unconjugated photosensitizer by gel filtration on Sephadex-G50 column (Pharmacia, Uppsala, Sweden) in the presence of 1.5 mol/L guanidine hydrochloride.

Binding of the MRTs by A431 cells. Fuctionality of the ligand module of the MRTs was tested by comparing the capacity of the MRTs to displace a truncated radiolabeled MRT, [^{125}I]iodo-DTox-HMP-EGF, from the surface of ErbB1 receptor overexpressing A431 cells. DTox-HMP-EGF and free EGF (Sigma) were [^{125}I]-iodinated (19) using 1,3,4,6-tetrachloro-3α-6α-diphenylglycouril (Sigma). The A431 cells were seeded at 250,000 per well in 48-well Costar plates (Corning, Corning, NY). After 24 hours, 20 nmol/L [^{125}I]iodo-HMP-NLS-EGF and serial dilutions of nonlabeled MRTs were added to the wells; the cells were incubated with ligands for 20 hours at 4°C. To minimize nonspecific binding, another MRT with different ligand module, DTox-HMP-NLS-MSH (9), was added in excess (2 μmol/L) to the incubation mixture. Cells were washed four times with cold Hanks' solution containing 10 mg/mL bovine serum albumin and 50 μg/mL gentamicin and lysed with 0.1 mol/L NaOH for 30 minutes. Radioactivity of the lysate was counted using RackBeta1217 scintillation counter (LKB, Uppsala, Sweden). Obtained results were corrected taking into account a nonspecific binding.

Interaction of the MRTs with α/β-importin heterodimer. pGEX2T-HA-PTAC97 plasmid encoding (glutathione *S*-transferase)-PTAC97 (β-importin) and pQE-IA plasmid encoding PTAC58 (α-importin) with hexaHis tag were kindly provided by Dr. Y. Yoneda (Osaka University, Japan) and Dr. V. Drutsa (Institute of Gene Biology RAS and Belozersky Institute of Physico-Chemical Biology, Moscow State University, Moscow, Russia), respectively. The importins were purified either on glutathion-Sepharose 4B (Pharmacia Biotech, Uppsala, Sweden), in the case of β-importin, or on Ni-NTA-agarose (QIAGEN), in the case of α-importin, and kept in 20% glycerol at −20°C. Equimolar concentrations of both importins were incubated in 20 mmol/L HEPES (pH 7.4) containing 110 mmol/L KCl, 5 mmol/L $NaHCO_3$, 5 mmol/L $MgCl_2$ (Sigma), 0.1 mmol/L $CaCl_2$ (Sigma), 1 mmol/L EGTA (Serva, Heidelberg, Germany), 1 mmol/L DTT (Fisher Scientific, Schwerte, Germany) to obtain importin heterodimer.

Surface plasmon resonance (SPR) experiments were done on BIACORE X equipment (BIACORE AB, Uppsala, Sweden). MRT under investigation was immobilized onto the sensor chip CM5 (BIACORE) with the Amine Coupling kit (BR-1000-50; BIACORE). Binding of the importin heterodimer to the MRT was measured by injecting a defined concentration of the heterodimer (within the 300 nmol/L to 1 μmol/L range) to the flow cell docking the MRT-immobilized sensor chip CM5 and loaded at a flow rate of 10 μL/min followed by a desorption step in the absence of the heterodimer. The chip was regenerated by injection of 30 μL of 10 mmol/L NaOH at a flow rate of 10 μL/min that completely removed all noncovalently bound proteins, this process did not change MRT affinity to the importin heterodimer (data not shown). The binding variables were computed by using the kinetic data analysis of the software (BIAevaluation 4.1) in the BIACORE system.

Interaction of the MRTs with small unilamellar liposomes and supported lipid bilayer at different pHs. Egg lecithin (KhimFarmZavod, Kharkov, Ukraine) was used without further purification. Small unilamellar vesicles were prepared according to Szoka and Papahadjopoulos (20) by sonicating fresh lipid suspension until clear, using a W-181-T sonicator (Finnsonik, Lahti, Finland; 40 kHz, 90 W, 0°C, 30 minutes), and passed several times through 0.45- and 0.22-μm filters (Corning). The liposomes were loaded with fluorescent calcein up to the concentration of fluorescence quenching, and its leakage under the MRT action at pH 3 to 7.5 was tested according to Rosenkranz et al. (21).

A Digital Instruments Multimode Scanning Probe Microscope on a Nanoscope IIIa (Veeco Instruments, Woodbury, NY) controller fitted with a 125-μm scanner (J-scanner) and a Tapping Mode liquid cell were used to image the lipid bilayer *in situ*. A piece of mica was attached to the 1.6-cm diameter metal disc supplied by Veeco and was installed in the microscope. The Tapping Mode liquid cell was fitted with inlet and outlet tubing to allow exchange of solutions in the cell during imaging. Samples of supported unilamellar bilayers were prepared by the vesicle fusion method as described by Puntheeranurak et al. (22). Briefly, a drop of about 100 μL of the lipid suspension (0.005-0.01 mg/mL) was applied to a piece of freshly cleaved mica, allowing incubation at room temperature for 15 minutes. Then the Tapping Mode liquid cell was sealed using a Teflon O-ring and flushed with fresh buffer [20 mmol/L HEPES, 20 mmol/L MES and 150 mmol/L NaCl (pH 7.5)] to remove any excess lipid before imaging. Specimens were imaged to check for bilayer. Oxide-sharpened silicon nitride V-shaped cantilevers with a nominal force constant of 0.06 N/m were used, and the forces were minimized during the scans. The cantilevers were irradiated with UV light before imaging to remove any adventitious

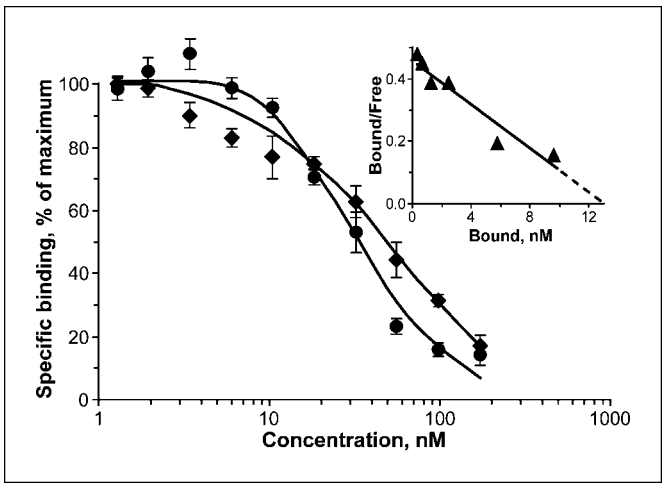

Figure 1. Displacement of [^{125}I]iodo-DTox-HMP-EGF (20 nmol/L) by DTox-HMP-NLS-EGF (●) and HMP-NLS-DTox-EGF (♦) from ErbB1 receptors of A431 human epidermoid carcinoma cells. A truncated MRT, [^{125}I]iodo-HMP-NLS-EGF, bound to A431 cell surface with dissociation constant of 110 nmol/L, number of binding sites was 3.1×10^6 per cell. *Inset,* [^{125}I]iodo-EGF binding to the A431 cells with dissociation constant of 28 nmol/L and 2.6×10^6 binding sites per cell.

organic contaminants. All measurements were done in contact and tapping modes (cantilever drive frequencies ~8.9 kHz) at room temperature using tip scan rate about 3 Hz. All images were captured as 512 × 512 pixel images and were flattened and smoothed.

Subcellular localization of the MRTs. A431 cells were incubated with 200 nmol/L MRT in DMEM containing 10% FCS for 4 hours, washed four times with Hanks' solution, and incubated in the serum-supplemented medium without MRT for 3 hours. Then the cells, washed four times with Hanks' solution, were fixed in cold (−20°C) methanol/acetone (2:3 v/v) mixture for 15 minutes. The fixed cells were permeabilized for 20 minutes at 35°C in 10 mmol/L HEPES (pH 7.3) containing 0.1% Tween 20 and 150 mmol/L NaCl (buffer A). After blocking with 5% fat-free dry milk in buffer A (40 minutes at 35°C), the cells were hybridized for 1 hour with affinity purified primary rabbit antibodies (1:100), raised by us against HMP-NLS-MSH polypeptide, in buffer A containing 5% fat-free dry milk and 5% goat serum (Sigma). The cells were washed four times with the buffer A, and after a second blocking with 5% fat-free dry milk in buffer A (20 minutes at 35°C), Cy-3-labeled anti-rabbit secondary antibodies (Sigma) were added for 1 hour with subsequent washing with the buffer A. To stain the cell nuclei, the cells were prelabeled with 1 μmol/L ToPro-3 (Molecular Probes, Eugene, OR) for 15 minutes (23). The cells were examined under TCS SP2 confocal laser scanning microscope with HCXPL APO CS ×100/1.4-0.7 objective, 1.4 numerical aperture (Leica Microsystems, Mannheim, Germany), at excitation and emission wavelengths corresponding to the dyes used.

Photocytotoxicity of photosensitizer-MRT conjugates. The A431 cells were seeded into 96-plates (2,000 per well); after 24 hours, they were incubated for 20 hours with photosensitizer or photosensitizer-MRT conjugates. The cells were washed thrice with Hanks' solution, placed into DMEM supplemented with 10% FCS for 3 hours, washed trice with Hanks' solution, placed into DMEM with 2 mg/mL bovine serum albumin, illuminated with a slide projector, 270 kJ/m^2 (100% cell survival without photosensitizers or photosensitizer-MRTs), and grown under 5% CO_2. Cell viability was determined in 3 to 4 days using methylene blue staining according to Finlay et al. (24).

Spin-trap assay of ROS production by a free and conjugated photosensitizer is described in the Supplementary Data.

Results

Design and production of the MRTs. We have produced two MRTs with the same modules: EGF, as a ligand module; DTox, translocation domain of diphtheria toxin, as an endosomolytic module; HMP, an *E. coli* hemoglobin-like protein, as a carrier module; and a modified NLS from SV40 large T-antigen, but differing in module localization in the polypeptide chain of the following MRTs: $(His)_6$-HMP-NLS-DTox-sp-EGF and $(His)_6$-DTox-HMP-NLS-sp-EGF [where sp, $(Gly\text{-}Ser)_5$ spacer] which will be designated further as HMP-NLS-DTox-EGF and DTox-HMP-NLS-EGF, respectively.

The HMP-NLS-DTox-EGF and DTox-HMP-NLS-EGF MRTs were obtained with ca. 80% and 98% purities, respectively. The first MRT turned out to be more susceptible to proteolysis in *E. coli* cells as was shown by Western blot which revealed hexaHis-tag containing products of the MRT degradation (data not shown).

Functionality of the MRT modules. The purified chimeric MRTs were tested to assess whether their individual modules retained their functional activities and were able to contribute to the overall goal of cell-specific nuclear photosensitizer delivery.

MRT binding by ErbB1 receptors was assessed using A431 human epidermoid carcinoma cells overexpressing ErbB1 receptors (25). Dissociation constants (K_d) for HMP-NLS-DTox-EGF and DTox-HMP-NLS-EGF, obtained from displacement curves (Fig. 1), were 40 ± 5 and 29 ± 4 nmol/L, respectively (mean ± SE), which are close to that for free [^{125}I]iodo-EGF (Fig. 1, *inset*; see also ref. 26).

MRTs delivered to cells by receptor-mediated endocytosis are internalized into endosomes (enclosed membranous structures with weakly acidic internal pH), which they must exit to be targeted subsequently to their final intracellular destination, in this case, the nucleus through the action of importins in the cytosol. The propensity of a polypeptide to make pores in membranes in an acidic medium can be assessed from its ability to effect leakage of dye-loaded liposomes at different pHs (27). Liposome leakage under the action of the MRTs (Fig. 2) was observed in two pH intervals: 3 to 4, which was attributable to the HMP because it alone showed a maximal activity at pH 3.5 to 4.5 (9), and 5.5 to 6.5, which is close to the endosomal pH (28), and was attributable to activity of the DTox moiety. Membrane defects produced by

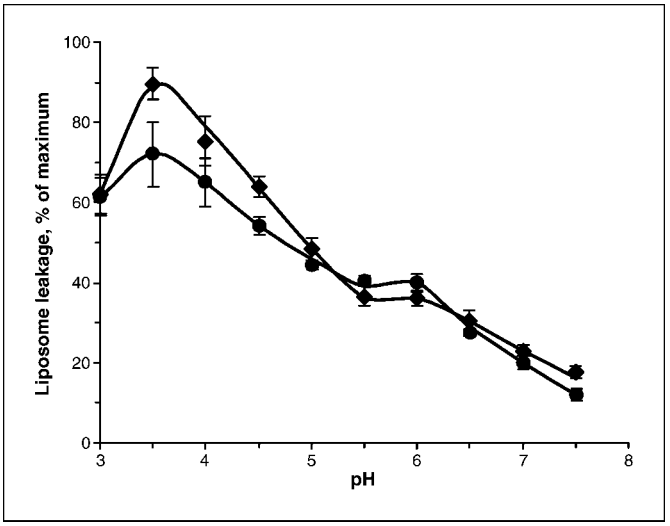

Figure 2. Liposome leakage induced by DTox-HMP-NLS-EGF (●) and HMP-NLS-DTox-EGF (♦). Egg yolk phosphatidylcholine liposomes were loaded with fluorescent calcein up to the concentration of fluorescence quenching; the liposome leakage resulted in appearance of fluorescence. *Points,* mean; *bars,* SE.

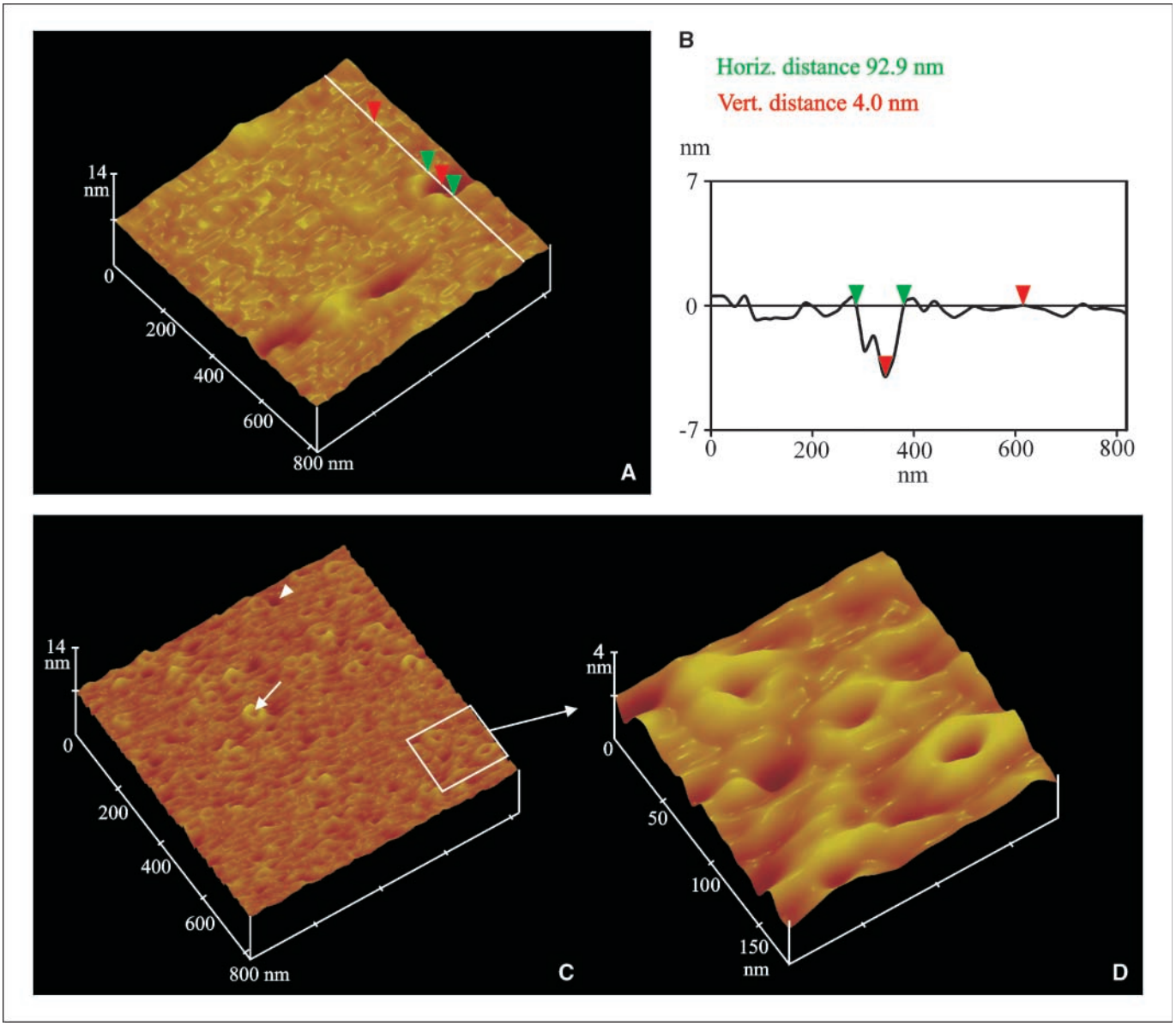

Figure 3. Hole formation in supported lipid bilayers induced by DTox-HMP-NLS-EGF at pH 5.5. *A,* atomic force microscopy contact mode height image (820 × 820 nm; *z*-scale, 14 nm) of egg yolk phosphatidylcholine bilayer recorded in 20 mmol/L HEPES-MES buffer with 150 mmol/L NaCl (pH 5.5) containing 10 nmol/L DTox-HMP-NLS-EGF. *B,* cross-section taken along the white line. Vertical and horizontal dimensions of the hole depth and width are measured between the red and green arrowheads, respectively. *C,* atomic force microscopy tapping mode height image of egg yolk phosphatidylcholine bilayer (820 × 820 nm; *z*-scale, 14 nm) and its zoom (*D*; 182 × 182 nm; *z*-scale, 4 nm) recorded in 20 mmol/L HEPES-MES buffer with 150 mmol/L NaCl (pH 5.5) containing 10 nmol/L DTox-HMP-NLS-EGF. One of the small depressions surrounded by a circular rampart is indicated by a white arrow, and one of the fluctuating holes is indicated by a white arrowhead.

DTox-HMP-NLS-EGF were assessed with the use of atomic force microscopy on supported egg lecithin bilayers (Fig. 3). At pH 5.5, the MRT caused formation of two types of defects in previously intact parts of the bilayer: (*a*) fluctuating holes (Fig. 3*A* and *C*, *arrowhead*) with typical diameters ranging from 10 to 150 nm and (*b*) structured small depressions or holes with mean diameter ± SE of 37 ± 2 nm (Fig. 3*C*, one of such holes is indicated by a white arrow, and Fig. 3*D*) surrounded by circular ramparts. The MRT did not cause the above-described defects at pH 7.5 (data not shown).

HMP-NLS-DTox-EGF and DTox-HMP-NLS-EGF MRTs were successfully immobilized on the BIACORE CM5 chips. The increments of SPR signal were about 10,700 and 4,000 RU, which corresponded to an immobilized MRTs of ca. 10.7 and 4.0 ng/mm^2, respectively. MRT-α/β-importin heterodimer interaction was well approximated with a two-state reaction model (29):

$$A + B \underset{k_{d1}}{\overset{k_{a1}}{\rightleftarrows}} AB \underset{k_{d2}}{\overset{k_{a2}}{\rightleftarrows}} AB^*,$$

where A and B are MRT and importin heterodimer, respectively; AB, their complex; AB*, the rearranged complex; k_{a1}, k_{a2} and k_{d1}, k_{d2}, association and dissociation rate constants, respectively, of corresponding states of the reaction; and $K_a = (k_{a1}/k_{d1}) \cdot (1 + k_{a2}/k_{d2})$, affinity constant. Assessment of the recognition of the MRTs by the nuclear transport-mediating α/β-importin heterodimer

Table 1. Association/dissociation rate constants and affinity constants (mean ± SE) of interaction of DTox-HMP-NLS-EGF and HMP-NLS-DTox-EGF MRTs with α,β-importin heterodimer assessed by SPR method

MRT	k_{a1} ($M^{-1}\cdot s^{-1}$)	k_{d1} (s^{-1})	k_{a2} (s^{-1})	k_{d2} (s^{-1})	K_a (M^{-1})
DTox-HMP-NLS-EGF	$(9.48 \pm 0.11) \times 10^3$	$(5.08 \pm 0.15) \times 10^{-3}$	$(2.81 \pm 0.12) \times 10^{-3}$	$(1.83 \pm 0.30) \times 10^{-4}$	3.06×10^7
HMP-NLS-DTox-EGF	$(1.75 \pm 0.04) \times 10^3$	$(6.08 \pm 0.05) \times 10^{-3}$	$(2.54 \pm 0.04) \times 10^{-3}$	$(4.76 \pm 0.44) \times 10^{-5}$	1.57×10^7

using an SPR assay indicated that the NLS in the context of the MRTs is able to interact with the importins. Both MRTs (HMP-NLS-DTox-EGF and DTox-HMP-NLS-EGF MRTs) revealed K_as of 1.6×10^7 and 3.1×10^7 L/mol, respectively (Table 1; Supplementary Fig. S1), very close to that for the same NLS as a free oligopeptide, 2.9×10^7 L/mol (29), and can be attributed to proteins with functional NLSs (30).

The MRTs were detected in A431 human epidermoid carcinoma cells with the use of indirect immunofluorescence microscopy. Figure 4 shows a predominant nuclear localization of DTox-HMP-NLS-EGF; HMP-NLS-DTox-EGF showed similar subcellular distribution (data not shown).

ROS production. Spin trapping of singlet oxygen and $^{\cdot}OH$ is considered as a convenient method for investigation of ROS generation in simple buffered water systems (31). The spin trapping of singlet oxygen with the use of 4-hydroxy-2,2,6,6-tetramethylpiperidine (TEMP) gives 4-hydroxy-2,2,6,6-tetramethylpiperidine-1-oxyl spin adduct (32). A typical triplet signal, with lines of equal intensities and 17.2 Gauss interspaces, appeared after illumination of aerated specimens containing bacteriochlorin *p* and TEMP; 10 mmol/L NaN_3 completely and competitively inhibited the adduct production suggesting involvement of singlet oxygen in the process. No signal was registered from nonilluminated specimens or specimens lacking bacteriochlorin *p* (Supplementary Fig. S2).

The second spin trap [5,5-dimethyl-1-pyrrolidine-*N*-oxide (DMPO)] can react with $^{\cdot}OH$, $^{\cdot}O_2^-$, and other radicals, giving rise to different spin adducts that can be identified according to their electron paramagnetic resonance (EPR) spectra (33). Illumination of aerated specimens containing DMPO and bacteriochlorin *p* resulted in multiplet EPR spectra. A quartet with line intensities 1:2:2:1 and 14.9 Gauss interspaces was attributed to DMPO-$^{\cdot}OH$ spin adduct. Ethanol (up to 50 mmol/L), used to verify participation of hydroxyl radicals in formation of the DMPO-$^{\cdot}OH$ adduct, caused a 3-fold reduction of the EPR signal of the adduct, whereas superoxide dismutase (20 μg/mL) caused only a 25% decrease of the signal suggesting inhibition of $^{\cdot}OH$ production by reactions (33) involving $^{\cdot}O_2^-$. Illumination of aerated specimens containing DMPO and nonconjugated MRT did not result in detectable nitroxyl radical signals (Supplementary Fig. S3).

Kinetics of formation of both adducts was registered at a fixed field strength corresponding to maximum of one of the characteristic lines. We did not reveal any significant variations in spin-adduct production kinetics between bacteriochlorin *p* covalently attached to MRT and free bacteriochlorin *p* (Supplementary Figs. S2*D* and S3*F*).

Photocytotoxicity of photosensitizers transported by the MRTs. Evaluation of the photocytotoxic effect on human A431 epidermoid carcinoma cells, which overexpress ErbB1 receptors, showed that the efficacy of photosensitizers is greatly enhanced by their attachment to MRTs in the case of both used photosensitizers chlorin e_6 (Fig. 5*A, C*, and *D*) and bacteriochlorin *p* (Fig. 5*B*). The most efficient (chlorin e_6)-DTox-HMP-NLS-EGF conjugate (EC_{50} = 0.53 nmol/L) displayed 3,360 times higher photocytotoxicity than free chlorin e_6 (EC_{50} = 1,780 nmol/L). (chlorin e_6)-HMP-NLS-DTox-EGF conjugate was less effective (EC_{50} = 2.25 nmol/L). Similar results showed (bacteriochlorin *p*)-HMP-NLS-DTox-EGF conjugate (EC_{50} = 4.2 nmol/L compared with 3,000 nmol/L for free bacteriochlorin *p*). Moreover, the MRTs impart cell specificity to photosensitizers: free chlorin e_6 is almost equally photocytotoxic for the cells overexpressing ErbB1 receptors (A431) and expressing a few (34) ErbB1 receptors (NIH 3T3 cells; Fig. 5*D*), whereas the same photosensitizer attached to the MRT was not photocytotoxic for non-target NIH 3T3 cells at the concentrations that were photocytotoxic for target A431 cells (Fig. 5*C*).

Discussion

Our experiments showed that the modules of the chimeric MRTs retain their functional activities. Interestingly, DTox included in different parts of the MRTs caused similar defects in lipid membranes, which suggests a possibility to use the DTox as an endosomolytic module in different polypeptide contexts, which agrees with findings made by Nizard et al. (35).

The main goal of this study was to show the possibility of ligand replacement. We used EGF as a ligand module because many tumor cell types (head-and-neck cancer, bladder cancer, carcinomas, gliosarcomas, breast cancer, etc.) overexpress ErbB1, or EGF receptors (13). Previously, we have shown that MSH-containing MRT could increase photosensitizer photocytotoxicity by 230-fold (9), whereas the present study with MRTs containing replaced ligand module (EGF instead of MSH) revealed a 3,000-fold increase. In both cases, photosensitizers transported by the MRT (in contrast to free photosensitizers) acquired cell specificity. Such a high

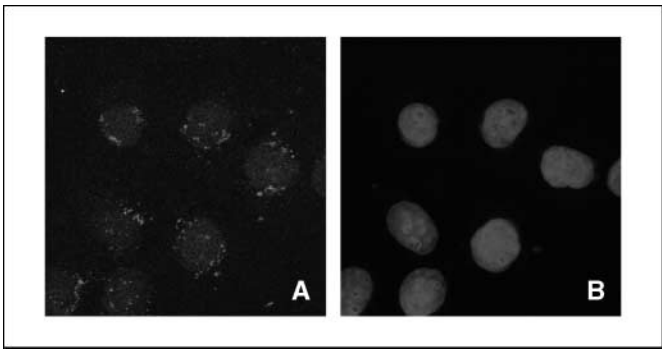

Figure 4. Subcellular localization of DTox-HMP-NLS-EGF in A431 human epidermoid carcinoma cells. The cells were incubated with 200 nmol/L MRT for 4 hours, then washed and incubated for 3 hours without the MRT, and then fixed and immunostained as described in Materials and Methods. The cell nuclei were prelabeled with 1 μmol/L ToPro-3. *A,* DTox-HMP-NLS-EGF. *B,* the same group of A431 cells, which nuclei are labeled with ToPro-3.

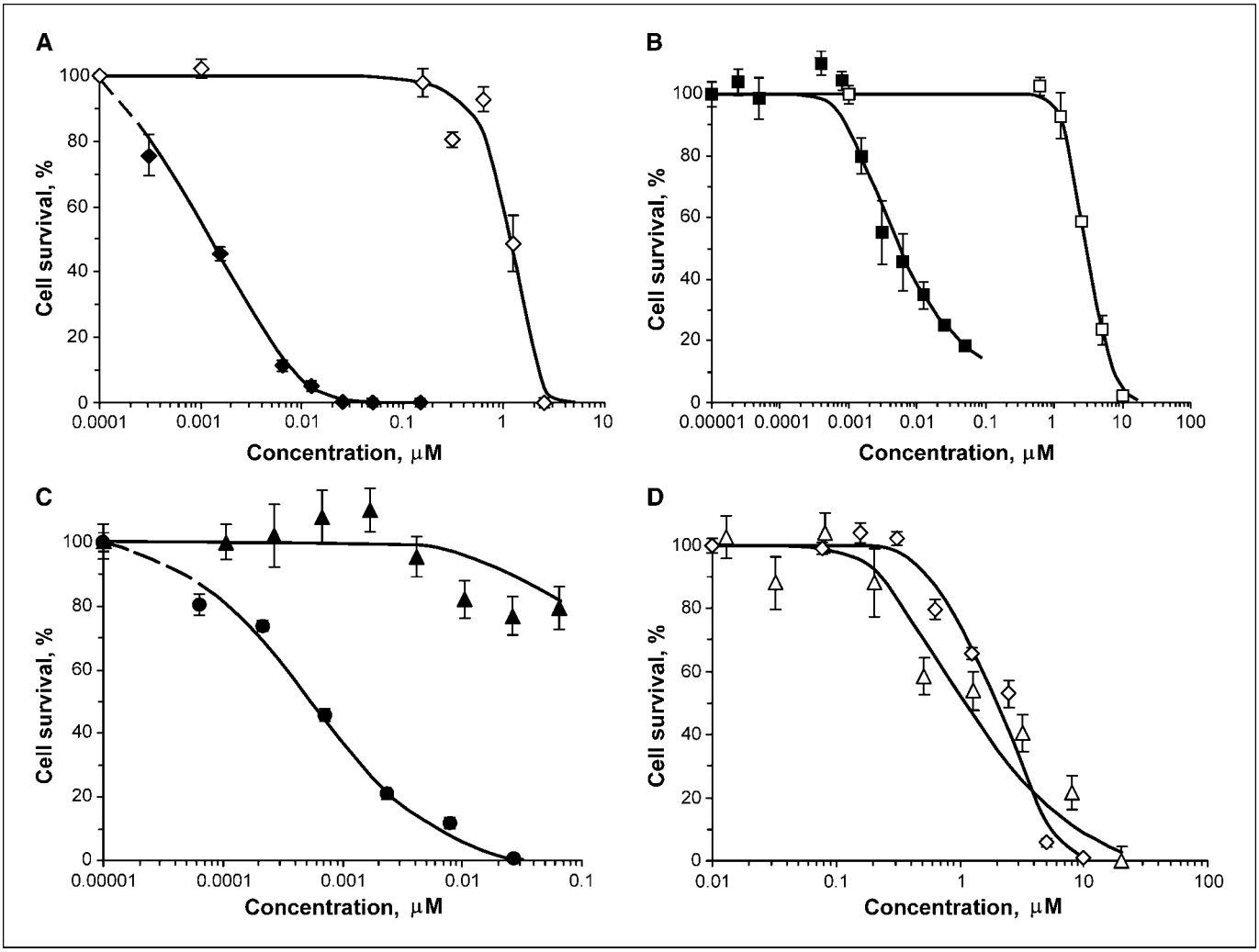

Figure 5. Photocytotoxicity of photosensitizer-MRT conjugates compared with free photosensitizers. *A,* (chlorin e_6)-HMP-NLS-DTox-EGF conjugate (♦) and free chlorin e_6 (◇). *B,* (bacteriochlorin *p*)-HMP-NLS-DTox-EGF conjugate (■) and free bacteriochlorin *p* (□). *C*, photocytotoxicity of (chlorin e_6)-DTox-HMP-NLS-EGF conjugate estimated on target A431 cells (●) and non-target NIH 3T3 cells (▲). *D*, photocytotoxicity of free chlorin e_6 estimated on target A431 cells (◇) and non-target NIH 3T3 cells (△). *Points,* mean; *bars,* SE.

photocytotoxicity can be attributed to intranuclear delivery of photosensitizers. Using just internalizable (chlorin e_6)-EGF conjugates and A431 cells, Gijsens et al. (36) showed 30 to 120 times less efficacy than our internalizable and intranuclearly deliverable (chlorin e_6)-MRT conjugates: EC_{50}s were 63, 2.25, and 0.53 nmol/L for (chlorin e_6)-EGF (36), (chlorin e_6)-HMP-NLS-DTox-EGF, and (chlorin e_6)-DTox-HMP-NLS-EGF (our data), respectively.

A relatively lower efficacy of (chlorin e_6)-HMP-NLS-DTox-EGF compared with that of (chlorin e_6)-DTox-HMP-NLS-EGF may be resulted from several causes (e.g., lower affinity to ErbB1 receptors and, possibly, higher intracellular degradability of the first MRT). These results show that an overall efficacy of an MRT may change as a result of module rearrangement, although every module retains, at least partially, its functionality after the rearrangement.

Our new MRTs have much higher killing effect compared with previously described MRTs (9), with >3,000 times greater efficacy than free photosensitizers versus >230 times (9), and can be used for treatment of a wider variety of cancers. Such a difference in efficacy may result from different number of corresponding overexpressed receptors in each study (ca. 10^4 and $>10^6$ receptors per B16-F1 melanoma and A431 carcinoma cell, respectively).

It is well known that melanoma is considered as an inappropriate tumor for photodynamic therapy treatment (2), owing to almost complete light absorption by melanin. Keeping in mind that our MSH-containing MRT gave ca. 230-fold enhancement of bacteriochlorin *p* efficacy (9) together with the fact that this photosensitizer possesses absorption peak at the wavelength (761 nm), where light penetration is better, we started *in vivo* experiments with this type of the MRTs.[5] The MSH-containing MRT given to C57/black mice bearing B16-F1 s.c. melanoma tumors selectively accumulated within the tumor cells and their nuclei even 3 hours after i.v. injection as was revealed with immunofluorescence microscopy. Bacteriochlorin *p* insignificantly ($P > 0.1$) influenced tumor growth and mean life span of the mice even after three administration/illumination cycles (two i.v. injections of

[5] P.V. Gulak, A.A. Rosenkranz, A.S. Sobolev, unpublished data.

0.014 mg/mouse with 24-hour interval, and the third one of 0.028 mg/mouse 2 days later, with subsequent illuminations, 360 J/cm^2 at 760 ± 10 nm, 3 hours after each injection), whereas this photosensitizer, used according to the same scheme and at the same doses but conjugated with the MRT, significantly ($P < 0.001$) increased mean life span of the mice (by 68 ± 4%) and inhibited tumor growth (9-day delay). The experiments with other photosensitizer-MRT administration/illumination schemes are still under way. We started *in vivo* experiments with EGF-containing MRTs described in this article, too, and believe that their *in vivo* efficacy would be greater not only because of higher *in vitro* efficacy but also because cancer cells overexpressing ErbB1 receptors are predominantly not pigmented.

MRTs of the type described here, capable of cell-specific targeting to particular subcellular compartments to increase photosensitizer efficacy, represent new pharmaceuticals with general application. The different modules of the MRTs, which are highly expressed and easily purified to retain full activity of each of the modules, are, of course, interchangeable, meaning that they can be tailored for particular applications; for example, ligands can be used depending on the desired target cell type.

Acknowledgments

Received 6/30/2006; revised 8/22/2006; accepted 8/30/2006.

Grant support: Dutch-Russian (NWO-RFFI) Scientific Cooperation grant 047.017.025 (A.S. Sobolev, A.A. Rosenkranz, P.V. Gulak, Y.V. Khramtsov, A.F. Mironov, and M.A. Grin), U.S. Civilian Research and Development Foundation grant RUB-02-2663-MO-05, and Russian Foundation for Basic Research grant 06-04-49273 (A.S. Sobolev, A.A. Rosenkranz, and P.V. Gulak).

The costs of publication of this article were defrayed in part by the payment of page charges. This article must therefore be hereby marked *advertisement* in accordance with 18 U.S.C. Section 1734 solely to indicate this fact.

We thank Dr. David J. Tremethick (J. Curtin School of Medical Research, Australian National University, Canberra, Australia) for critical reading of the article, Dr. Y. Yoneda (Osaka University, Japan) for the pGEX2T-HA-PTAC97 plasmid encoding glutathione *S*-transferase-(β-importin), and Olga Vorontsova and Elena Artemenko for assistance with confocal microscopy and EPR spectrometry, respectively.

References

1. Dolmans DE, Fukumura D, Jain RK. Photodynamic therapy for cancer. Nat Rev Cancer 2003;3:380–7.
2. Brown SB, Brown EA, Walker I. The present and future role of photodynamic therapy in cancer treatment. Lancet Oncol 2004;5:497–508.
3. Sobolev AS, Jans DA, Rosenkranz AA. Targeted intracellular delivery of photosensitizers. Prog Biophys Mol Biol 2000;73:51–90.
4. Rosenkranz AA, Jans DA, Sobolev AS. Targeted intracellular delivery of photosensitisers to enhance photodynamic efficiency. Immunol Cell Biol 2000;78:452–64.
5. Sharman WM, van Lier JE, Allen CM. Targeted photodynamic therapy via receptor mediated delivery systems. Adv Drug Deliv Rev 2004;56:53–76.
6. Akhlynina TV, Jans DA, Rosenkranz AA, et al. Nuclear targeting of chlorin e_6 enhances its photosensitizing activity. J Biol Chem 1997;272:20328–31.
7. Akhlynina TV, Jans DA, Statsyuk NV, et al. Adenovirus synergize with nuclear localization signals to enhance the nuclear delivery and photodynamic action of internalizable conjugates containing chlorin e_6. Int J Cancer 1999;81:734–40.
8. Sobolev AS, Akhlynina TV, Rosenkrants AA, Jans DA. Composition and method for causing photodynamic damage to target cells. United States patent 6,500,800. 2002.
9. Rosenkranz AA, Lunin VG, Gulak PV, et al. Recombinant modular transporters for cell-specific nuclear delivery of locally acting drugs enhance photosensitizer activity. FASEB J 2003;17:1121–3.
10. Rosenkranz AA, Nabatnikov PA, Aliev RA, Jans DA, Sobolev AS. [Enhancement of a cytotoxic effect by targeted transport of α-emitter Astatine-211 into human hepatoma cell nuclei.] Molekulyarnaya Meditsina [Molecular Medicine, Moscow] 2004;2:47–55 [in Russian].
11. Ouban A, Muraca P, Yeatman T, Coppola D. Expression and distribution of insulin-like growth factor-1 receptor in human carcinomas. Hum Pathol 2003;34:803–8.
12. Schramm A, Schulte JH, Astrahantseff K, et al. Biological effects of TrkA and TrkB receptor signaling in neuroblastoma. Cancer Lett 2005;228:143–53.
13. Mendelsohn J, Baselga J. The EGF receptors family as targets for cancer therapy. Oncogene 2000;19:6550–65.
14. Reubi JC, Macke HR, Krenning EP. Candidates for peptide receptor radiotherapy today and in the future. J Nucl Med 2005;46 Suppl 1:S67–75.
15. Salazar-Onfray F, Lopez M, Lundqvist A, et al. Tissue distribution and differential expression of melanocortin 1 receptor, a malignant melanoma marker. Br J Cancer 2002;87:414–22.
16. Lunin VG, Sergienko OV, Khodun M-VL, Bader LB, Karpov VA, Tikhonenko TI, inventors. Method of preparing of recombinant plasmids $pC(Sp)_nS$ encoding chimeric protein with somatostatin sequence. Russian patent 2,031,121. 1995.
17. Laemmli UK. Cleavage of structural proteins during the assembly of the head of bacteriophage T4. Nature 1970;227:680–5.
18. Mironov AF, Kozyrev AN, Brandis A. Sensitizers of second generation for photodynamic therapy of cancer based on chlorophyll and bacteriochlorophyll derivatives. Proc SPIE 1992;1922:204–8.
19. Fraker PJ, Speck JC, Jr. Protein and cell membrane iodinations with a sparingly soluble chloroamide, 1,3,4,6-tetrachloro-3α,6α-diphenylglycouril. Biochem Biophys Res Commun 1978;80:849–57.
20. Szoka F, Jr., Papahadjopoulos D. Procedure for preparation of liposomes with large internal aqueous space and high capture by reverse-phase evaporation. Proc Natl Acad Sci U S A 1978;75:4194–8.
21. Rosenkranz AA, Antonenko YN, Smirnova OA, Yurov GK, Naroditsky BS, Sobolev AS. Avian adenovirus induces ion channels in model bilayer lipid membranes. Biochem Biophys Res Commun 1997;236:750–3.
22. Puntheeranurak T, Stroh C, Zhu R, Angsuthanasombat C, Hinterdorfer P. Structure and distribution of the *Bacillus thuringiensis* Cry4Ba toxin in lipid membranes. Ultramicroscopy 2005;105:115–24.
23. Haugland RP. Handbook of fluorescent probes and research products. 9th ed. Gregory J, editor. Molecular Probes, Eugene: 2002. p. 338–42.
24. Finlay GJ, Baguley BC, Wilson WR. A semiautomated microculture method for investigating growth inhibitory effects of cytotoxic compounds on exponentially growing carcinoma cells. Anal Biochem 1984;139:272–9.
25. Lokeshwar VB, Huang SS, Huang JS. Protamine enhances epidermal growth factor (EGF)-stimulated mitogenesis by increasing cell surface EGF receptor number. Implications for existence of cryptic EGF receptors. J Biol Chem 1989;264:19318–26.
26. Kawamoto T, Sato JD, Le A, Polikoff J, Sato GH, Mendelsohn J. Growth stimulation of A431 cells by epidermal growth factor: identification of high-affinity receptors for epidermal growth factor by an anti-receptor monoclonal antibody. Proc Natl Acad Sci U S A 1983;80:1337–41.
27. Nir S, Nieva JL. Interactions of peptides with liposomes: pore formation and fusion. Progr Lipid Res 2000;39:181–206.
28. Ceresa BP, Schmid SL. Regulation of signal transduction by endocytosis. Curr Opin Cell Biol 2000;12:204–10.
29. Catimel B, Teh T, Fontes MR, et al. Biophysical characterization of interactions involving importin-α during nuclear import. J Biol Chem 2001;276:34189–98.
30. Hodel MR, Corbett AH, Hodel AE. Dissection of a nuclear localization signal. J Biol Chem 2001;276:1317–25.
31. Horikoshi S, Hidaka H, Serpone N. Hydroxyl radicals in microwave photocatalysis. Enhanced formation of OH radicals probed by ESR techniques in microwave-assisted photocatalysis in aqueous TiO_2 dispersions. Chem Phys Lett 2003;376:475–80.
32. Misra BR, Misra HP. Vasoactive intestinal peptide, a singlet oxygen quencher. J Biol Chem 1990;265:15371–4.
33. Das KS, Misra HP. Scavengers of hydroxyl radicals and inhibitors of NADPH-dependent lipid peroxidation in bovine lung microsomes. J Biol Chem 1992;267:19172–8.
34. Di Fiore PP, Pierce JH, Fleming TP, et al. Overexpression of the human EGF receptor confers an EGF-dependent transformed phenotype to NIH 3T3 cells. Cell 1987;51:1063–70.
35. Nizard P, Chenal A, Beaumelle B, Fourcade A, Gillet D. Prolonged display or rapid internalization of the IgG-binding protein ZZ anchored to the surface of cells using the diphtheria toxin T domain. Protein Eng 2001;14:439–46.
36. Gijsens A, Missiaen L, Merlevede W, de Witte P. Epidermal growth factor-mediated targeting of chlorin e_6 selectively potentiates its photodynamic activity. Cancer Res 2000;60:2197–202.

Targeting Cancer Cells by Novel Engineered Modular Transporters

Dinara G. Gilyazova, Andrey A. Rosenkranz, Pavel V. Gulak, et al.

Cancer Res 2006;66:10534-10540.